Bureau of Mines Report of Investigations/1983

Corrosion of Selected Metals and a High-Temperature Thermoplastic in Hypersaline Geothermal Brine

By R. K. Conrad, J. P. Carter, and S. D. Cramer

UNITED STATES DEPARTMENT OF THE INTERIOR

Report of Investigations 8792

Corrosion of Selected Metals and a High-Temperature Thermoplastic in Hypersaline Geothermal Brine

By R. K. Conrad, J. P. Carter, and S. D. Cramer

UNITED STATES DEPARTMENT OF THE INTERIOR
James G. Watt, Secretary

BUREAU OF MINES
Robert C. Horton, Director

This publication has been cataloged as follows:

Conrad, R. K. (Regis K.)

Corrosion of selected metals and a high-temperature thermoplastic in hypersaline geothermal brine.

(Report of investigations ; 8792)

Supt. of Docs. no.: I 28.23:8792.

1. Corrosion and anti-corrosives. 2. Thermoplastics—Corrosion. 3. Geothermal brines. 4. Geothermal power plants—Equipment and supplies—Corrosion. I. Carter, J. P. (John P.). II. Cramer, Stephen D. III. Title. IV. Series: Report of invesrigations (United States. Bureau of Mines) ; 8792.

TA462.C617 1983 620.1'623 83-600111

CONTENTS

ILLUSTRATIONS

TABLES

UNIT OF MEASURE ABBREVIATIONS USED IN THIS REPORT

A	ampere	MPa	megapascal
cm	centimeter	mV	millivolt
°C	degree Celsius	μm	micrometer
kPa	kilopascal	μm/a	micrometer per year
L	liter	ohm-cm^2	ohm-square centimeter
L/h	liter per hour	pct	percent
L/min	liter per minute	ppm	part per million
m	meter	V	volt
mA/cm^2	milliampere per square centimeter	V/h	volt per hour
mg	milligram	vol pct	volume percent
min	minute	wt pct	weight percent
mm	millimeter		

CORROSION OF SELECTED METALS AND A HIGH-TEMPERATURE THERMOPLASTIC IN HYPERSALINE GEOTHERMAL BRINE

By R. K. Conrad,[1] J. P. Carter,[2] and S. D. Cramer[3]

ABSTRACT

The Bureau of Mines conducted corrosion research to determine suitable construction materials for geothermal resource recovery plants. Weight loss, pitting and crevice corrosion, U-bend stress corrosion, and electrochemical polarization measurements were made on selected metals in brine and steam process environments produced from high-enthalpy hypersaline brine from geothermal well Magmamax No. 1 at the Salton Sea Known Geothermal Resources Area, Imperial Valley, Calif.

Cadmium (and by extension cadmium coatings) and a 6061-T6 aluminum alloy were unsatisfactory because of high general corrosion rates and, in the case of aluminum, severe pitting. Molybdenum and niobium (columbium) were resistant to general corrosion, pitting, and crevice corrosion. Copper alloys corroded at rates that may preclude their use in wellhead brine. The presence of iron accelerated the corrosion of the copper alloys. Titanium alloys were resistant to general corrosion and stress corrosion cracking in all of the environments. They exhibited crevice corrosion in some of the brine and steam environments and Ti6Al4V pitted in the brine environments. They exhibited passive behavior over a broad range of potentials.

Exposure tests were conducted on a high-temperature polyphenylene sulfide thermoplastic (Ryton) in the same environments. A 40-pct-graphite-fiber-reinforced Ryton composite deteriorated readily in wellhead brine and failed in all of the brine and steam process environments; Ryton coatings on 316L stainless steel were adherent and performed well.

[1]Chemist.
[2]Research chemist.
[3]Supervisory chemical engineer.
All authors are with the Avondale Research Center, Bureau of Mines, Avondale, Md.

INTRODUCTION

As part of the U.S. Department of the Interior, Bureau of Mines, effort to promote the wise and efficient use of domestic mineral resources (2, 6, 12, 17, 19),[4] various materials of construction have been evaluated in hypersaline geothermal brines from the Imperial Valley, Calif., for use in geothermal resource recovery plants. These brines contain high levels of dissolved salts, 20 wt pct or more, largely as alkali and alkaline-earth metal chlorides (8-9), and dissolved gases such as CO_2, NH_3, CH_4, and H_2S. Downhole temperatures may exceed 300° C, and wellhead pressures range up to 2.5 MPa.

The brine and steam process streams produced from high-enthalpy hypersaline geothermal brines can be highly corrosive. The Bureau's research on corrosion in geothermal brines has consisted of both laboratory (8-9) and field studies (3-5). The present work reports some of the results for a large field test involving weight-loss measurements of up to 45-day duration on more than 20 commercial and experimental alloys and a high-temperature thermoplastic in brine and steam environments, stress corrosion tests on many of the metals, and electrochemical corrosion measurements on 45 commercial and experimental alloys in wellhead brine. Only the results of the measurements on Cu and Ti alloys, Al 6061-T6, Mo, Nb, and Cd, and the high-temperature thermoplastic are reported here.

Titanium and copper alloys are widely used in corrosive service applications. Molybdenum and niobium may find applications as structural materials or as cladding in critical components such as pumps, valves, screens, or bearings. Cadmium coatings on steel exhibit somewhat better corrosion resistance than zinc coatings in marine atmospheric exposures (16), and there was interest in their performance in geothermal environments. A high-temperature polyphenylene sulfide, having the trade name Ryton[5] and the chemical formula $(-C_6H_4S-)_n$, was used previously in the Bureau's laboratory as a coating to protect steel autoclave components for short times (less than 5 days) from corrosion in hypersaline geothermal brine at 232° C. While the operating temperature of corrosion test packages in the field test was higher than the maximum recommended temperature for use of Ryton in a graphite-fiber-reinforced composite, 150° C (1), it was less than the highest working temperature reported for the thermoplastic, 230° to 260° C (14-15).

ACKNOWLEDGMENT

The authors gratefully acknowledge the contributions of samples for inclusion in these studies by Babcock and Wilcox, Advanced Composites Department, Alliance, Ohio (40-pct-graphite-fiber-reinforced polyphenylene sulfide composite); Astro Metallurgical Corp., Columbus, Ohio; Kawecki Berylco Industries, New York, N.Y., and H. M. Hillman Brass and Copper Inc., Willow Grove, Pa.

[4]Underlined numbers in parentheses refer to items in the list of references at the end of this report.

[5]Use of trade names is for identification purposes only and does not imply endorsement by the Bureau of Mines.

EXPERIMENTAL PROCEDURE

Corrosion tests were conducted in brine and steam process streams produced by flash evaporation of wellhead brine from geothermal well Magmamax No. 1 at the Bureau of Mines geothermal test facility on the Salton Sea Known Geothermal Resources Area (KGRA) in the Imperial Valley, Calif. Figure 1 is a block diagram of the facility and shows the relative locations of the test packages for the corrosion measurements. The operation of the facility is described in RI 8350 (5). Weight-loss corrosion measurements and U-bend stress corrosion tests were made in wellhead brine and in the brine and steam process streams from the two steam separators. Electrochemical potentiodynamic and linear polarization measurements were made in wellhead brine only in a separate test package operated in parallel to the weight-loss wellhead brine test package P1.

The operating conditions for each test package, averaged over the approximately 45 days the test facility was in operation, are given in table 1. Included in this table are the pH (measured at 25° C) and chloride concentration of the brine and of the condensed steam from the five process streams. The flow of wellhead brine into weight-loss wellhead brine test package P1 averaged 130 L/min. The steam separators each produced brine enriched in salts and an impure steam that contained some entrained salts. The temperature and pressure of the brine and steam process streams were the same at their exit from the brine separators, and the two streams were thus considered to be at equilibrium.

The chloride content of the brines increased with each separation owing to evaporative losses of water. Chloride was present in the steam because of liquid carryover in the form of spray or mist. Separator 1 was operated so that there was more carryover than from separator 2 and, hence, the steam from separator 1 had a higher salt content.

The brine pH increased with each separation because the noncondensable acidic gases CO_2 and H_2S were stripped from the brine. These gases were evidently lost when the steam was condensed, as the condensed steam had a higher pH than that of the brine. Scale formed on the metal samples in each corrosion test package. The composition and mineralogy of the scale, while not considered in this report, was shown to be a function of the environment in earlier work (5).

TABLE 1. - Operating conditions for corrosion test packages[1]

Corrosion test packages	Temp., °C	Absolute pressure, MPa	pH	[Cl-], ppm
P1 and electrochemical package 1 (wellhead brine).....	215	2.00	5.3	115,000
P2 (brine from separator 1).....	199	1.63	5.7	127,000
P3 (steam from separator 1).....	199	1.63	6.2	8,100
P4 (brine from separator 1).....	180	1.02	5.8	129,000
P5 (steam from separator 2).....	180	1.02	6.9	1,700

[1]Input flow rate = 130 L/min.

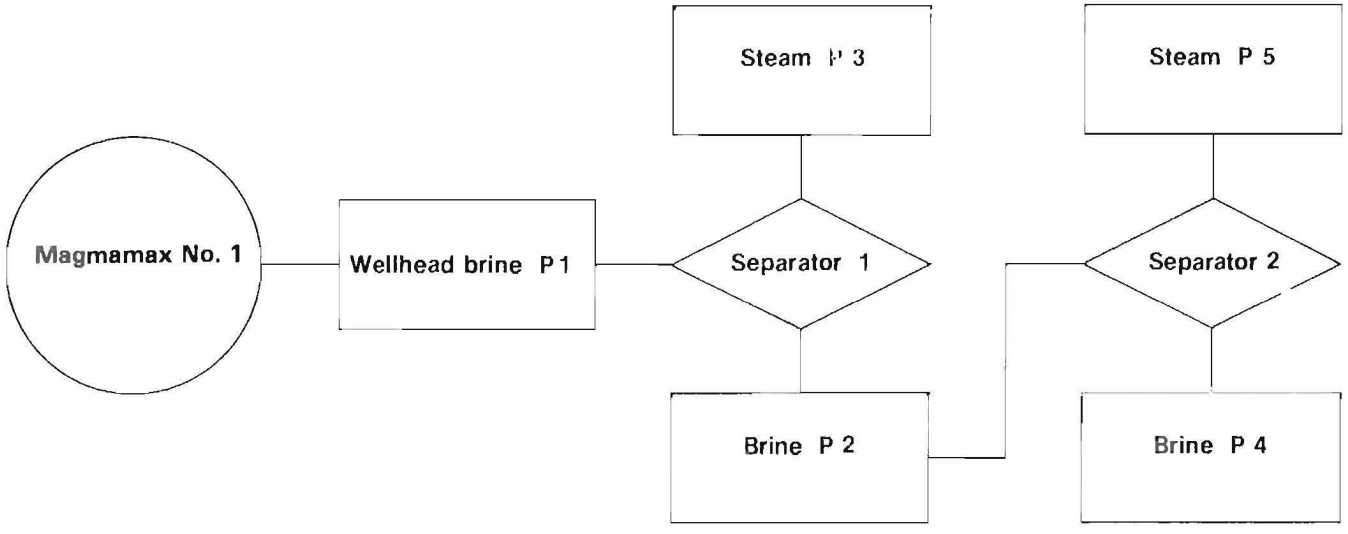

FIGURE 1. - Block diagram of the Bureau of Mines geothermal test facility showing location of corrosion test packages (P1-P5).

WEIGHT-LOSS AND LOCALIZED CORROSION TESTS

Weight-loss corrosion tests were conducted on the titanium alloys Ti50A, TiCode 12, and Ti6Al4V, and on Mo, Nb, and Cd. Compositions of these metals are given in tables 2 and 3. A high-temperature polyphenylene sulfide thermoplastic, used both as a coating on 316L stainless steel (SS) and as part of a graphite fiber reinforced composite, also was exposed in these tests.

Metal test samples, 25 by 44 mm, were sheared from a 1.6- to 3.2-mm-thick sheet. A 6.4-mm-diam mounting hole was punched in the center of the 25-mm side, and the center of the hole was 6.4 mm in from the edge. The sample edges and the holes were lightly ground to remove metal distorted by shearing. The samples were degreased with methanol in an ultrasonic cleaner, washed with ASTM No. 1 water, dried in warm air, and weights were recorded to within ±0.1 mg.

TABLE 2. - Titanium alloy compositions, weight percent

Alloy	Al	C	Fe	Other
Ti50A.....	0	0.008	0.03	0.20 O.
Ti0.2Pd.....	0	.009	.13	0.20 Pd, 0.14 O.
TiCode 12.....	0	0	.31	0.44 Mo, 0.86 Ni.
Ti6Al4V.....	6.4	.042	.15	4.08 V, 0.15 O.
Ti6Al2Nb1TalMo.....	6.0	(1)	(1)	2.0 Nb, 1.0 Ta, 0.8 Mo.

[1]Not measured.

NOTE.--Balance is titanium.

TABLE 3. - Other metal compositions, weight percent

Metal	Ni	Ta	Ti	Zn	Other
Cd.....	0	0	0	0.02	Balance Cd.
Mo.....	.1 max	0	.01 max	0	Balance Mo.
Nb.....	0	.3 max	.03 max	0	Balance Nb.

Ryton-coated 316L SS samples were prepared in the following way. Substrate pretreatment was exactly as described for the metal weight-loss samples, with the exception that the sample surface was sandblasted with clean glass beads, 200-325 mesh, prior to degreasing. A primer, CorroTherm CT-33, was sprayed onto the substrates as an aqueous slurry to a thickness of approximately 0.02 mm. The primer was air cured at 375° for 15 min. The Ryton coating was applied as multiple layers of equal thickness over the primer. Each layer was sprayed onto the substrate as an 80-pct aqueous slurry of clear, unpigmented Ryton to a thickness of approximately 0.1 mm. Each layer was air cured at 375° C for 15 to 20 min. A total of five layers was applied for a final coating thickness of 0.5 mm. The final layer was air cured at 375° C for 60 min. The curing conditions for the primer and for the Ryton coatings were determined by consultation with the manufacturers of the products and by limited laboratory testing to develop the coatings procedure.

The 40-pct-graphite-fiber (Thornel 300) reinforced Ryton composite samples were cut to the same size as the metal weight-loss samples. They were 2.4 mm thick. The mounting hole was in the same position as on the metal weight-loss samples. The samples were degreased with methanol, rinsed with ASTM No. 1 water, and air dried. Neither these samples nor the Ryton-coated stainless steel samples were weighed since the evaluation of the exposed samples was to be done optically with a microscope.

The test samples were mounted, as shown in figure 2, on support rods for exposure to the process environments in the corrosion test packages. Four samples each of the three titanium alloys (only two were cleaned for weight-loss measurements) were mounted on the support rods. The other samples were used for experiments not covered by this report. Single Mo, Nb, Cd, graphite-fiber-reinforced Ryton, and Ryton-coated 316L SS samples were mounted on the support rods on a space-available basis and, hence, only a few tests of each were made in the various

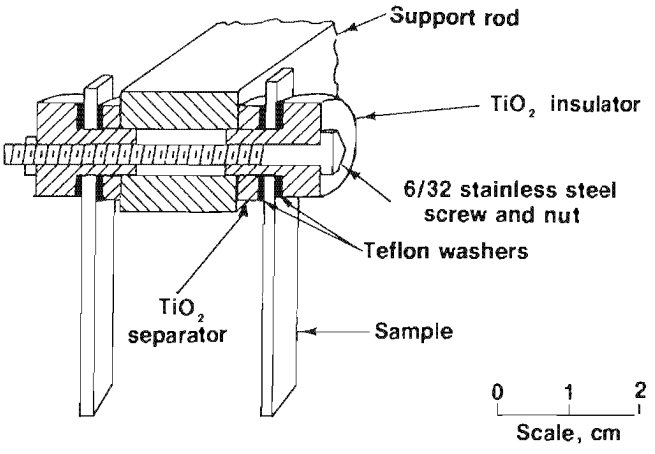

FIGURE 2. - Weight-loss corrosion sample mounting assembly.

process environments. The 2.4-m-long support rods were axially loaded into one of four sections of the corrosion test package, as shown in figure 3. The details of the sample mounting and corrosion test package loading are given in RI 8350 (5). During the 45-day operation of the test facility, six test packages were exposed, one for 45 days, one for 30 days, and four separate packages for 15 days. All of the Ryton-coated 316L SS samples were exposed for 15 days and graphite-fiber-reinforced Ryton samples were exposed 45 days.

At the end of each exposure period, the appropriate support rods were removed from the corrosion test packages and carefully rinsed with water to remove soluble salts from the samples. The rods and associated samples were air dried before being shipped to the Bureau's laboratory for cleaning and evaluation.

The scale covering each of the samples varied from hard and thick to thin and powdery, depending upon the package from which the sample was removed. Cleaning of the samples involved mechanical removal of as much of the scale as possible by chipping or brushing. The remainder of the scale was removed chemically by immersing the samples in a stripping solution. Scale was removed from the niobium, Ryton, and titanium alloy samples by immersing them for 2 to 10 min in 20 vol pct nitric acid at 60° C. When the scale was particularly difficult to

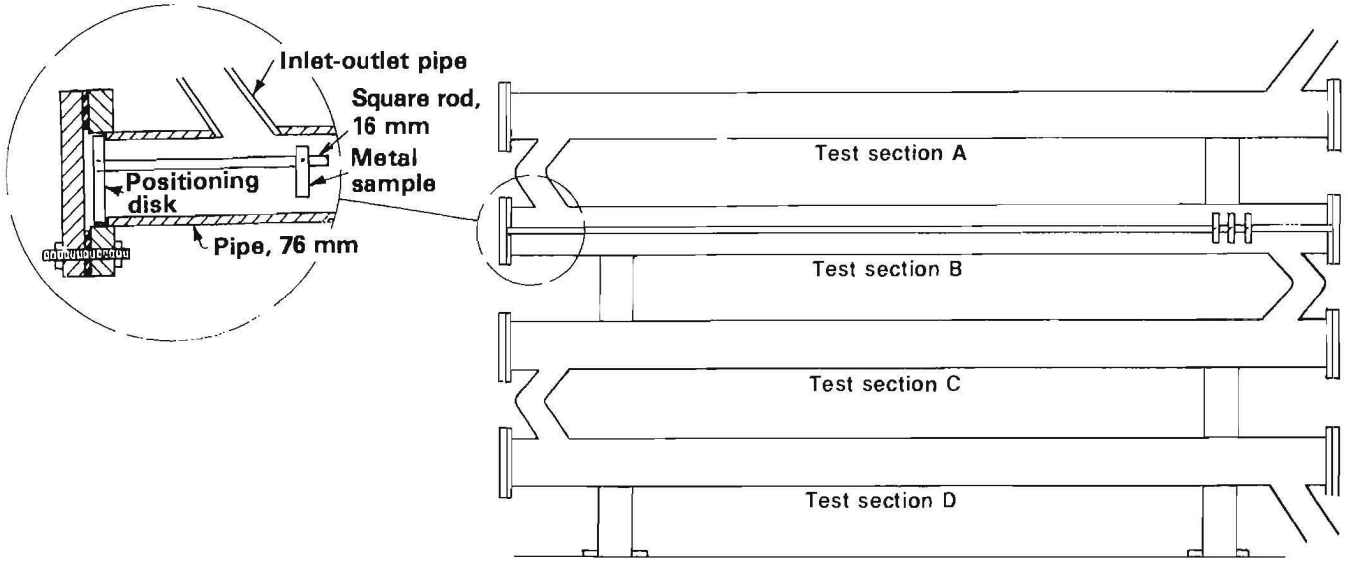

FIGURE 3. - Weight-loss corrosion test package.

remove, 2 to 5 drops of HF were added to this solution.

Scale was removed from the molybdenum samples by immersing them in concentrated HCl at room temperature for 2 to 5 min. The cleaned samples were rinsed with ASTM No. 1 water and dried in warm air. The weights of the metal samples were then recorded to within ±0.1 mg, and general corrosion rates were calculated from the sample weight loss. The maximum metal loss from the samples during the chemical removal of scale was determined from blanks exposed to the stripping solutions for typical cleaning times. The metal loss from these blanks was converted into an equivalent loss in sample thickness corresponding to the three test periods. These values, expressed in micrometers per year, are given in table 4 and correspond to the general corrosion rate detection limits.

The metal samples were examined with a microscope for evidence of pitting and crevice corrosion. The depth of attack was measured using an optical micrometer. While the precision of the optical micrometer was ±2.5 μm, the minimum pit depth that could be resolved by this technique and, hence, the pit detection limit, was 13 μm.

TABLE 4. - General corrosion rate detection limits based upon metal loss from blanks treated in typical cleaning cycles, micrometers per year

Exposure period, days.....	15	30	45
Mo.....	0.4	0.2	0.1
Nb.....	.3	.2	.1
Ti50A.....	1.9	.9	.6
Ti6Al4V.....	4.8	2.4	1.8
TiCode 12.....	6.5	3.2	2.2

Pitting rates were computed from the measured pit depths and the sample exposure time. Pitting rates are reported as both maximum rates and average rates. The former were computed from the greatest pit depth, while the latter were computed from the average for the 10 deepest pits. However, for multiple tests, such as the four 15-day tests, the maximum rate was the highest value observed in any of the four tests, while the average rate was the mean of the averages computed in each test.

The Ryton samples were examined with a microscope for damage to the coating, such as cracking and blistering, and to the composite, such as debonding of the graphite fibers from the Ryton matrix.

U-bend stress corrosion tests of 45-day duration were conducted on the titanium alloys (Ti50A, TiCode 12, and Ti6Al4V). The rectangular U-bend samples, measuring 25 by 102 mm, were sheared from 1.6- to 3.2-mm-thick alloy sheet. A 6.4-mm-diam mounting hole was punched near each end of the sample, and the edges and holes were lightly ground on a wet belt sander to remove burrs and metal distorted by shearing. The samples then were bent into the U-bend configuration on a mandrel having a 13-mm radius of curvature. After bending, all of the samples were prepared by (1) degreasing in methanol, (2) ultrasonic rinsing in tapwater fol lowed by distilled water, and (3) drying in warm air. The U-bend samples were not weighed since previous work (9) had shown that general corrosion rates were similar for the U-bend samples and unstressed samples.

The corrosion test packages and support rods used in the weight-loss measurements also were used for the U-bend stress corrosion tests. The sample mounting procedure was similar, except that the legs of the U-bend samples were mounted on opposite sides of the support rod with the appropriate ceramic insulators, spacers, and Teflon washers (fig. 2). Half as many U-bend samples could be mounted on a support rod as weight-loss samples. The U-bend samples were exposed to wellhead brine and to brine and steam process streams from the two steam separators for 45 days.

At the completion of the stress corrosion tests, the samples were unloaded from the corrosion test packages, rinsed with water, and dried. Subsequently they were returned to the Bureau's laboratory for cleaning and evaluation. The samples were cleaned following the same procedure used for the weight-loss samples. After cleaning, they were visually examined under a low power (X 10 to X 60) microscope for stress corrosion cracks in the U-bend area. If none were observed, the legs of the U-bend sample were closed by crimping them together and the sample was reexamined for cracks that may have been exposed. If still none were observed, the sample edges were then examined at higher magnification on a metallograph.

ELECTROCHEMICAL MEASUREMENTS

Electrochemical potentiodynamic and linear polarization measurements were made on cylindrical electrodes of the copper alloys 70-30 cupronickel, 90-10 cupronickel, naval brass, Berylco 50, and Berylco 717; the titanium alloys Ti50A, Ti0.2Pd, Ti6Al4V, and Ti6Al2NblTalMo; and 6061-T6 aluminum. The compositions of these alloys are given in tables 2, 5, and 6. The cylindrical electrodes were fabricated from rod and were 6 to 10 mm in diameter and 18 to 42 mm long. One end of each electrode was drilled to a depth of 13 mm and tapped for a 5-40 thread. The electrodes were mechanically ground to a 240-grit surface finish with silicon carbide abrasive, washed in distilled water, rinsed with methanol, and dried in warm air.

The electrodes were mounted on a Petrolite M-511E industrial probe rated for use at 4.1 MPa and 260° C and designed for insertion and retraction of the probe head under pressure using a packing gland and an extension shaft. The electrodes were screwed in place on threaded-pin electrical feed throughs (5-40 thread size) installed in the probe head by special glass-metal seals. A size 2-006 Viton-A O-ring, placed between the electrode and the glass-metal seal, formed a leak-tight seal surrounding the threaded-pin electrical feed throughs, which eliminated electrochemical interferences which otherwise would occur as a result of brine contacting the feed throughs. Three electrodes (working, counter, and reference) were mounted on the probe head.

TABLE 5. - Copper alloy compositions, weight percent

Alloy	Be	Fe	Zn	Ni	Other
Naval brass.....	0	0.1	35.4	0	0.2 Pb, 0.8 Sn.
Berylco 50.....	.42	0	0	0	1.05 Ag, 1.59 Co.
Berylco 717.....	.5	.7	0	31	None.
70-30 cupronickel....	0	1.0-1.8	1.0	30	1.0 Mn.
90-10 cupronickel....	0	.4- .7	1.0	10	1.0 Mn.

NOTE.--Balance is copper.

TABLE 6. - 6061-T6 aluminum alloy composition, weight percent

Cr..	0.03-0.04	Si..	0.04-0.8
Cu..	.15- .40	Ti..	.15 max
Fe..	.7 max	Zn..	.25 max
Mg..	.8 -1.2	Al..	Balance
Mn..	.15 max		

The industrial probe was mounted in the electrochemical package shown in figure 4. At the time of mounting, the probe was in the retracted position, the 0.4-L probe chamber was empty of brine, and the 51-mm gate valve was closed. The corrosion package test section contained hot flowing brine. The probe chamber was filled by first slightly and then fully opening the gate valve while simultaneously venting residual air and then steam and brine from the chamber. After filling the probe chamber with brine, venting continued at a rate of 5 to 10 L/h. At this rate, the brine in the probe chamber was replaced with fresh brine in 5 min or less.

The corrosion test section (used with the electrochemical package) and the electrochemical package were wrapped with an approximately 15.2-cm-thick layer of fiberglass insulation to minimize heat losses and maintain the brine at a constant temperature. Measurements of the brine temperature in the probe chamber, when vented at a rate of 5 to 10 L/h and also after a 20-min period when venting was stopped and the 2-in gate valve was closed, were identical with the wellhead brine temperature, 215° C.

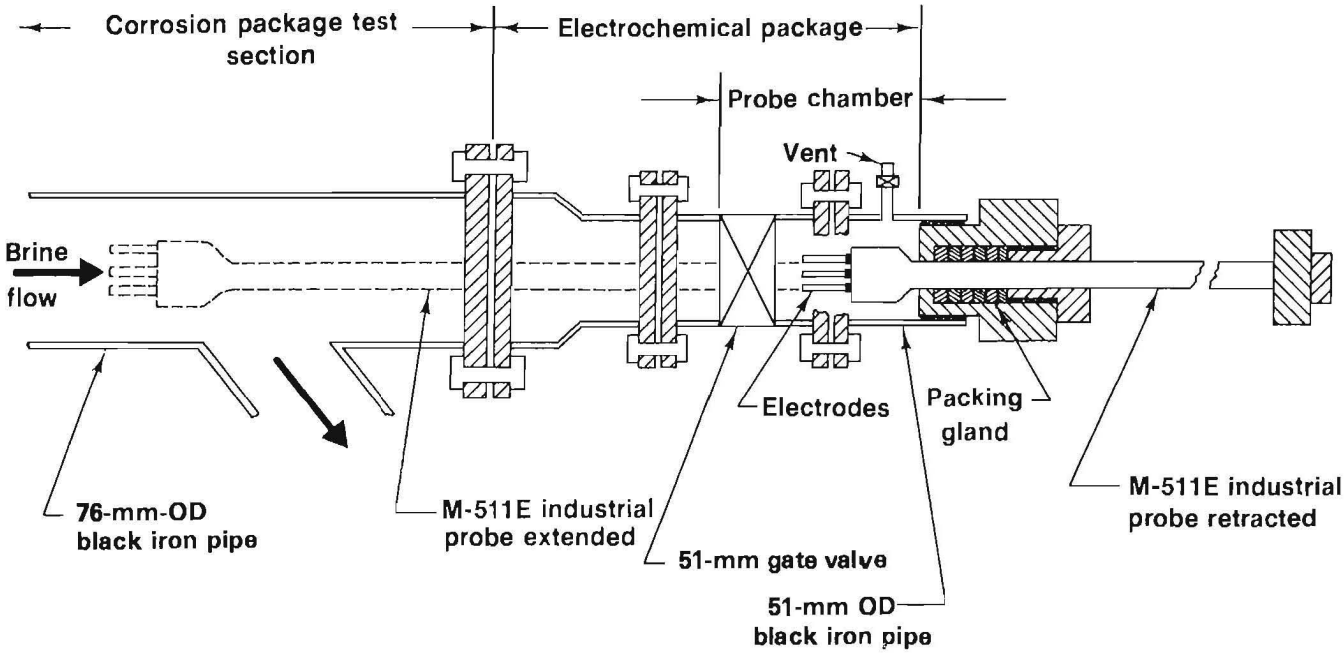

FIGURE 4. - Electrochemical corrosion test package.

Linear Polarization Measurements

Three-point linear polarization measurements (7) were used to obtain corrosion rates by the technique described in RI 8308 (10). Measurements were made with the Petrolite M-511E probe in the retracted position so that the head of the probe was totally within the probe chamber. Venting of the brine from the probe chamber was stopped and the 51-mm gate valve was closed immediately before each measurement to prevent interference from pressure fluctuations due to control operations elsewhere in the test facility. Following each measurement, the gate valve was reopened and venting of the probe chamber resumed.

The current source for the measurements was a Petrolite M-103E portable corrosion rate instrument modified for independent measurement of current and potential. The current was measured by a Keithley 616 electrometer in series with the counter electrode. The potential between the working and reference electrode was measured by a Keithley 616 electrometer. The reference electrode was a freely corroding electrode of the same material as the working electrode. The working, counter, and reference electrodes were fabricated from the same alloy, had identical dimensions, and were surface prepared and cleaned in the same way.

A measurement consisted of a pair of cathodic and anodic current readings obtained at -10 and +10 mV from the corrosion potential. Such measurements were made at roughly 5-min intervals over a 30-min period after the probe chamber was filled with brine. Since a galena-based scale forms on metals exposed to the wellhead brine, the cathodic and anodic currents for a "scale-free" working electrode, i_c and i_a, were obtained by the procedure described earlier (10). In this procedure, the current-time data were extrapolated to time zero to obtain the values for the condition when the working electrode was known to be free of scale. All tests were run in duplicate, and the averages of the scale-free anodic and cathodic currents were used to determine the corrosion current. The corrosion current, expressed as a current density in amperes per square centimeter, j_{corr}, was estimated from the three-point linear polarization equation (7) as

$$j_{corr} = \frac{1}{2.3} \frac{(b_a b_c)}{b_a+b_c} \frac{(i_c+i_a)}{2\Delta\phi A}, \qquad (1)$$

where b_a and b_c are the anodic and cathodic Tafel constants, in millivolts per decade, i_a and i_c are the absolute value, in amperes, of the scale-free anodic and cathodic currents measured at +10 and -10 mV from the corrosion potential; $\Delta\phi$ is the absolute value of the polarization, 10 mV; and A is the surface area of the working electrode in square centimeters. Values of the Tafel constants were not known, but $(b_a b_c)/(b_a+b_c)$ is roughly 50 mV for many systems and was assumed to be that value here. Furthermore, the polarization resistance in ohm-square meters, R_p, was estimated from the three-point linear polarization equation (7) as

$$R_p = \frac{2\Delta\phi A}{1{,}000(i_c+i_a)}. \qquad (2)$$

The corrosion rate, r, expressed in micrometers of electrode surface thickness lost per year, was computed by combining equation 1 with Faraday's law to give

$$r = 3.268 \times 10^6 \frac{j_{corr}(M/z)}{\rho}, \qquad (3)$$

where M is the atomic weight of the metal, z is the valence change during dissolution of the metal, and ρ is its density, in grams per cubic centimeter. Weighted values of the ratio M/z and of ρ, determined by the mass fraction of each alloy constituent, were used for alloys in equation 3.

At the conclusion of the 30-min measurement period, the gate valve was closed, and the vent was fully opened to exhaust steam from the probe chamber until the chamber pressure was reduced to

101 kPa. The M-511E probe was then removed from the electrochemical package, and the electrodes visually inspected, both for surface condition and for leaks around the Viton-A O-rings. Tests were repeated in the few cases where leaks were discovered.

Potentiodynamic Polarization Measurements

Potentiodynamic polarization measurements were made using an AIS model PEC-1B potentiostat and Wenking VSG-72 scan generator. Current and voltage were measured using Keithley 616 electrometers. Log current-voltage data were plotted on X-Y coordinates using an AIS model PEC-LM logarithmic converter. Electrodes were mounted on a Petrolite M-511E industrial probe as in the linear polarization measurements. The reference electrode was a freely corroding electrode of the same material as the working electrode. The working, counter, and reference electrodes were fabricated from the same alloy, had identical dimensions, and were surface prepared and cleaned in the same way. The resulting polarization curves could not be related to a thermodynamically defined potential scale because of the choice of reference electrode; however, the shape of the polarization curves and important features related to active-passive dissolution, susceptibility to pitting and crevice corrosion, and metal repassivation were obtained by this procedure.

Measurements were made with the Petrolite M-511E probe in the retracted position. Measurements began 10 min after the brine was admitted to the probe chamber. Immediately before the measurements, the probe chamber vent and then the 51-mm gate valve were closed. The measurements consisted of a single scan beginning 500 to 1,000 mV cathodic to the open circuit potential, E_{corr}, and swept in the anodic direction through E_{corr} and into the transpassive region at a rate of 60 V/h. The scan direction was reversed in the transpassive region when the anodic current had increased an order of magnitude above the passive current or when the anodic current reached 1 A. The reverse scan was continued until the current changed from anodic to cathodic. Less than 4 min were required to complete a scan. At the conclusion of the scan, the vent was opened to reduce the probe chamber pressure to 101 kPa and the M-511E probe was removed. After checking the electrodes for leaks around the Viton-A O-rings, the electrodes were rinsed in distilled water to remove dissolved salts, and were dried and stored for later examination.

RESULTS AND DISCUSSION

WEIGHT-LOSS AND LOCALIZED CORROSION TESTS

General Corrosion

General corrosion rates for Mo, Nb, and Cd, determined from the limited 15-, 30-, or 45-day weight-loss tests in the brine and steam process environments, are given in table 7. All of the measured rates are above the detection limits given in table 4. The rates for molybdenum and niobium in brine and steam process environments produced from Magmamax No. 1 geothermal brine are low, roughly 20 to 30 times smaller than the value of 50 μm/a used by industry in assigning an "ideal" rating to material that exhibits essentially no dimensional change during the life of the process (11). The cadmium samples, on the other hand, completely dissolved during the tests, and cadmium-coated steel is clearly unsuitable for these environments.

The general corrosion rates for Ti50A, TiCode 12, and Ti6Al4V determined from weight-loss tests in the brine and steam process environments are also given in table 7. The rates for the 30- and 45-day exposures are the average from two samples each, and rates for the 15-day exposure are the average from eight samples (two samples in each of four 15-day tests). All measured rates equivalent to or less than the detection limits given

TABLE 7. - General corrosion rates for Mo, Nb, and Cd, and titanium alloys in brine and steam process environments produced from Magmamax No. 1 geothermal well, micrometers per year

Exposure, days	P1	P2	P3	P4	P5
Molybdenum:					
15	1.6	NT	3.5	NT	1.4
30	NT	NT	NT	NT	3.4
45	NT	0.9	NT	0.3	NT
Niobium:					
15	NT	.8	NT	NT	NT
30	NT	NT	1.0	NT	NT
45	.4	.2	NT	.8	NT
Cadmium:					
15	NT	[1]>31,000	NT	NT	NT
30	NT	NT	NT	NT	NT
45	NT	NT	[1]>10,000	NT	NT
Ti50A:					
15[2]	0	0	0	0	0
30	46	0	0	0	0
45	20	0	5.1	0	0
TiCode 12:					
15[2]	0	0	0	0	0
30	0	0	0	0	0
45	0	0	0	0	0
Ti6Al4V:					
15[2]	107	0	0	0	0
30	86	0	0	0	0
45	160	0	0	0	0

NT Not tested.
P1 Wellhead brine.
P2 1st separated brine.
P3 1st separated steam.
P4 2d separated brine.
P5 2d separated steam.
[1]Sample dissolved during test.
[2]Mean of four 15-day tests.

NOTE.--All measured rates equivalent to or less than general corrosion rate detection limits (table 4) are reported as zero.

in table 4 are reported as zeros. All of the titanium alloys were resistant to general corrosion in the separated brine (P2 and P4) and steam (P3 and P5) packages. These data also show that Ti50A and TiCode 12 are both resistant to corrosion in wellhead brine and that TiCode 12 gives somewhat better performance than Ti50A. The Ti50A data are in good agreement with earlier laboratory weight-loss measurements in deaerated Salton Sea KGRA-type geothermal brine at 232° C (9), and field linear polarization measurements in wellhead brine at 229° C (10). The TiCode 12 data agree with earlier field weight-loss data for wellhead brine (5). The data for Ti6Al4V indicate that this alloy is less resistant to corrosion in wellhead brine than either Ti50A or TiCode 12 and that it tends to corrode at a rate greater than the ideal rating.

The Ryton-coated 316L SS samples exposed 15 days were examined under a low power (X 10 to X 60) microscope for failure in the coatings. Separations of the coating from the 316L SS substrate and blisters were observed in samples exposed to wellhead brine (P1) and brine from the second separator (P4). The coating edges were chipped on samples exposed to brine and steam from the first separator (P2 and P3) and to steam from the second separator (P5). In general, however, the coatings on these samples were very adherent. The varied results in packages P1 and P4, as compared with P2, P3, and P5, point toward the possibility of inconsistent coating technique as a cause of the occasional coatings failure due to blistering. It should be possible to correct this application problem, and the results suggest that Ryton

coatings have potentially useful applications in high-temperature geothermal brine environments.

Photomacrographs of the 40-pct-graphite-fiber-reinforced Ryton composite exposed 45 days in brine and steam process environments and cleaned to remove scale deposits are shown in figure 5, along with a photomacrograph of the unexposed material. All photomacrographs were taken at the same magnification. Samples exposed to wellhead brine (P1) suffered large losses of matrix material (Ryton) everywhere on the surface, exposing the graphite-fiber reinforcement. Cracks formed in the composite parallel to the exposed graphite fibers, and some fibers debonded (separated) from the matrix. Samples exposed to the brine and steam from the first and second separators were damaged substantially less

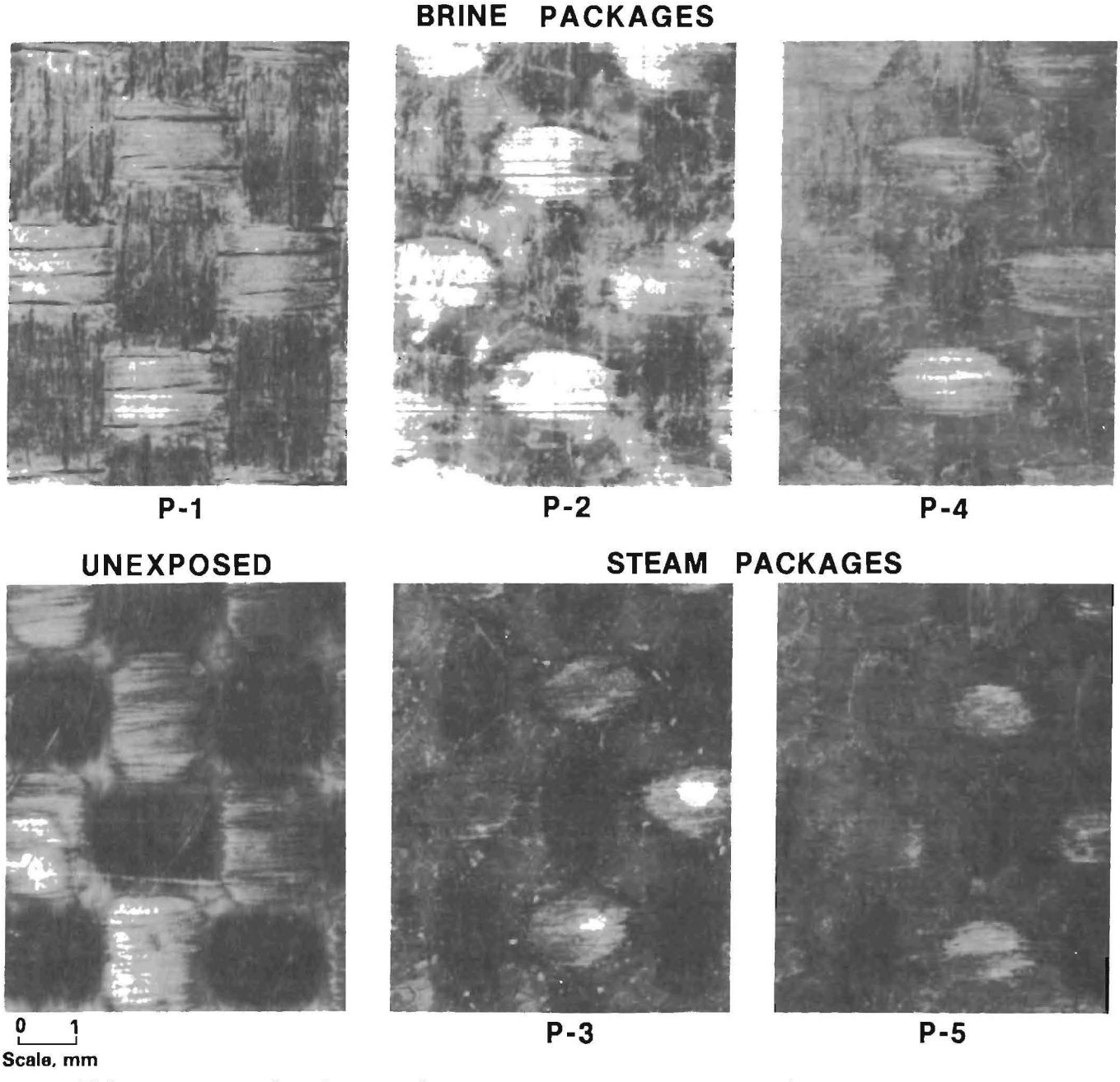

FIGURE 5. - Graphite-fiber-reinforced Ryton composites exposed 45 days in brine and steam corrosion test packages.

than those exposed to wellhead brine. There was some loss of matrix material from the surface, but cracks in the composite parallel to the fiber reinforcement were the principal form of damage. Cracking and debonding probably resulted from the use of the graphite-fiber-reinforced Ryton composite at temperatures considerably above the maximum recommended temperature, 150° C (1). The loss of matrix material from the sample surface would seem to involve other factors as well, such as erosion.

Localized Corrosion

No evidence of pitting or crevice corrosion was found on the molybdenum or niobium samples exposed to the wellhead brine and to the separated brine and steam process environments. None of the titanium alloys exposed 45 days to the wellhead brine and the separated brine and stream process environments showed any evidence of stress corrosion cracking. A number of titanium alloy samples exhibited evidence of crevice corrosion. It appeared as accelerated corrosion in and about the crevice formed between the Teflon washer and the sample in the mounting assembly (fig. 2). This was observed on Ti50A in wellhead brine and brine and steam from separator 1 (P1, P2, and P3), on Ti6Al4V in wellhead brine and brine from separator 1 (P1 and P2), and on TiCode 12 in the two separated brine environments (P2 and P4).

Pitting corrosion rates for the three titanium alloys are reported in table 8 for the five brine and steam process environments. The data are reported as maximum and average pitting rates in micrometers per year. The minimum pit depth that could be resolved by the optical micrometer was 13 μm, equivalent to detection limits for the different exposure periods, in micrometers per year, of 15 days--330, 30 days--160, and 45 days--110. However, defects in the form of irregularities in the surface of unexposed titanium alloy samples led to some detection limits that were higher. These detection limits were measured by an optical micrometer in the same way as pit depths. Maximum and average values of the defect depth, representing the deepest defects and the average of the 10

TABLE 8. - Maximum and average pitting rates for titanium alloys in brine and steam process environments produced from Magnamax No. 1 geothermal well, micrometers per year

Exposure, days	P1	P2	P3	P4	P5
Ti50A					
15:					
Maximum.....	670	0	0	0	0
Average[1].....	0	0	0	0	0
30:					
Maximum.....	0	0	0	0	0
Average.....	0	0	0	0	0
45:					
Maximum.....	0	0	0	0	0
Average.....	0	0	0	0	0
TiCODE 12					
15:					
Maximum.....	0	540	0	0	0
Average[1].....	0	355	0	0	0
30:					
Maximum.....	0	0	0	580	0
Average.....	0	0	0	290	0

Exposure, days	P1	P2	P3	P4	P5
TiCODE 12--Con.					
45:					
Maximum.....	0	150	0	0	0
Average.....	0	0	0	0	0
Ti6Al4V					
15:					
Maximum.....	1,200	740	0	0	0
Average[1].....	0	0	0	0	0
30:					
Maximum.....	480	860	0	0	0
Average.....	240	190	0	0	0
45:					
Maximum.....	0	0	0	0	0
Average.....	0	0	0	0	0

P1 Wellhead brine. P3 1st separated steam. P5 2d separated steam.
P2 1st separated brine. P4 2d separated brine. [1]Mean of four 15-day tests.

NOTE.--Only pitting rates that exceed detection limits for maximum and average pitting and corrosion rates (table 9) are reported; lower values are reported as zero.

deepest defects, were determined. These limits, expressed in terms of pitting rates for the different exposure periods, in micrometers per year, are given in table 9. Only pitting rates that exceed the detection limits given in table 9 are reported in table 8. All other values are reported as zero.

TABLE 9. - Detection limits for maximum and average pitting corrosion rates based upon the measurement of defect depths and roughness in the surface of unexposed samples, micrometers per year

Exposure, days	Ti50A	TiCode 12	Ti6Al4V
15:			
Maximum.....	590	330	650
Average.....	460	330	330
30:			
Maximum.....	290	160	320
Average.....	225	160	160
45:			
Maximum.....	195	110	215
Average.....	150	110	110

The data for Ti50A and TiCode 12 suggest that pitting is not a problem in the wellhead brine or in the separated brine and steam process environments. Except for one value in table 8, Ti50A showed no evidence of pitting corrosion. This agrees with earlier laboratory experiments in a Salton Sea KGRA-type brine at 215° C containing dissolved methane (100 ppm) or dissolved carbon dioxide (250 ppm), where the pitting rate for Ti50 was below the detection limit (8). Pitting rates for TiCode 12 in the two separated brines (P2 and P4) are somewhat higher than the detection limit. These values represent pits that formed in the crevice area of the TiCode 12 samples and, hence, are due solely to the presence of the crevice. Thus, it is apparent that Ti50A and TiCode 12 are not susceptible to pitting attack in the brine or steam process environments.

The data for Ti6Al4V indicate that it is susceptible to pitting corrosion in the wellhead brine (P1) and in the brine from the first separator (P2). Although the average pitting rates are at or near the detection limits, the maximum pitting rates are substantially higher and indicate that a few deep pits are prone to form in Ti6Al4V. The existence of only a few deep pits suggests that pit nucleation does not readily occur on Ti6Al4V in these environments. The maximum pitting rate declines substantially with increased exposure time. This decrease is most likely due to the deposition of scale on the metal surface so as to restrict access of the brine to the pits and, hence, retard propagation. No pitting of Ti6Al4V occurred in the two steam environments (P3 and P5) or in the brine from separator 2 (P4).

ELECTROCHEMICAL MEASUREMENTS

Linear Polarization Measurements

Linear polarization measurements on five copper alloys, four titanium alloys, and one aluminum alloy in wellhead brine at 215° C are summarized in table 10. The polarization resistance was computed using equation 2, and the corrosion rate computed using equation 3. The polarization resistance values are included in table 10 because assumptions about the values of the Tafel constants are not used in their computation.

The general corrosion rates of the copper alloys varied by a factor greater than 20. Stepwise multiple regression analysis was used to determine which of the alloy constituents from among Be, Fe, Ni, and Zn had a significant effect on the corrosion rate. The effect of the few "other" elements shown in table 5 was not considered. A total of 10 data points was available since each value in table 10 is the average of two measurements. The common logarithm of the corrosion rate, r (in micrometers per year), was correlated with various linear combinations of the alloying element concentrations. The null hypothesis that the coefficients in this analysis were zero was tested at the 0.10-level of significance using a t-test. The presence of Be, Ni, and Zn was shown not to contribute significantly to the general corrosion of the copper alloys in wellhead

TABLE 10. -- Linear polarization measurements in wellhead brine at 215° C

Alloy	Polarization resistance (Rp), ohm-cm^2	General corrosion rate, μm/a
Copper:		
Naval brass.....	347	1,005 ± 140
Berylco 50.....	259	755 ± 5
Berylco 717.....	238	1,055 ± 230
70-30 cupronickel.....	145	1,775 ± 350
90-10 cupronickel.....	344	730 ± 25
Titanium:		
Ti50A.....	6,900	27.4± .7
Ti0.2Pd.....	2,620	71.9± 11.1
Ti6Al4V.....	14,500	13.0± 1.1
Ti6Al2NblTalMo.....	22,400	8.4± .3
Aluminum: 6061-T6.....	4.6	51,000 ±14,500

brine. On the other hand, the presence of iron in the copper alloys was strongly correlated with their corrosion performance. This relationship was described by the equation

$$\log_{10} r = 2.87743 + 0.21963\ [Fe], \quad (4)$$

where [Fe] is the concentration of iron in the copper alloy, expressed in weight percent. Clearly the presence of iron increases the general corrosion rate of the copper alloys compared with those that are free of iron. The general corrosion rate for iron-free copper, as determined by the constant in equation 4, is 754 μm.

The general corrosion rates of the titanium alloys varied by a factor of 8 and are 10 to 200 times lower than the values obtained for the copper alloys. Contrary to what might be expected, the corrosion rate for Ti0.2Pd was higher than for Ti50A. This may be due to the higher iron content of the Ti0.2Pd alloy. Additions of aluminum combined with other alloying elements resulted in corrosion rates that were substantially lower than for Ti50A. For example, Ti6Al4V corroded at a rate half that of Ti50A, and Ti6AlNblTalMo corroded at a rate one-third that of Ti50A. The addition of Nb, Ta, and Mo in combination appears to be more effective in reducing the corrosion rate than the corresponding addition of vanadium.

Given the uncertainty in comparing results in two separate but similar tests, the general corrosion rate obtained by linear polarization for Ti50A compares reasonably well with the earlier reported value obtained by linear polarization, 5.3 μm/a (10). The polarization resistance value of 6,900 ohm-cm^2 compares well with the mean of the three values reported by Syrett (18) of 6,500 ohm-cm^2, obtained from laboratory measurements in a Salton Sea KGRA-type brine at pH 5.4 and 250° C.

The general corrosion rates obtained for Ti50A and Ti6Al4V by linear polarization would appear to contradict the ranking of these materials as indicated by the weight-loss results reported in table 7. However, linear polarization was used here to obtain an instantaneous measure of the corrosion rate under scale-free conditions after only a short exposure to the brine, while the weight-loss procedure measured the corrosion rate in a relatively long exposure to the brine under scaling conditions. When pitting is not a factor, as in the case of Ti50A, the linear polarization results would appear to reflect the actual corrosion rate of the material when free of scale other than the corrosion product. This value then constitutes an upper limit, and the value from the weight-loss results, representing the time average of the corrosion rate as scale deposits on the metal surface and access of the

brine to the surface is restricted, would lie below this value. The results for Ti50A appear to agree with such an interpretation.

When a metal is susceptible to localized corrosion, as in the case of Ti6Al4V in wellhead brine, interpretation of the results is more complex. The metal loss due to pitting, and perhaps to a lesser extent crevice corrosion, in the weight-loss test substantially outweighs the loss due to general corrosion as measured by linear polarization. Thus, while the linear polarization measurements suggest Ti6Al4V is more resistant to general corrosion than Ti50A, when localized corrosion effects are combined with general corrosion in the long-term weight-loss tests, Ti50A appears to be the more corrosion-resistant material.

The corrosion rate of the 6061-T6 aluminum alloy was roughly estimated at 51,000 μm/a. The alloy pitted severely during the linear polarization measurements, and a heavy white corrosion product surrounded the pits. These results are not surprising since laboratory tests in a Salton Sea KGRA-type brine (9) and a field test at the East Mesa KGRA (13) both have shown that aluminum alloys experience severe general corrosion and pitting in high-enthalpy, low- and high-salinity geothermal brines.

Potentiodynamic Polarization Measurements

Potentiodynamic polarization test results for the copper and titanium alloys in wellhead brine at 215° C are summarized in table 11. Critical current densities for the copper and titanium alloys ranged from 9 to 18 mA/cm^2 while passive current densities ranged from 1 to 7 mA/cm^2. The passive current densities are less than an order of magnitude smaller than the corresponding critical current densities. This represents an extremely narrow range of values, considering the widely different corrosion behaviors of the copper and titanium alloys and the fact that the linear polarization measurements showed up to a 200-fold variation in their corrosion rate. It suggests the possibility for solution species electrochemical reactions occurring simultaneously with the metal dissolution reaction.

Electrochemical reactions of solution species can have the effect of yielding polarization curves that are quite different from those for the metal dissolution reaction alone. However, there has been no work on the electrochemistry of high-temperature, hypersaline geothermal brines that would help in the interpretation of the potentiodynamic polarization curves. Consequently, they will be

TABLE 11. - Potentiodynamic polarization measurements in wellhead brine at 215° C

Alloy	Active-passive behavior	Susceptible to localized corrosion	Current density, mA/cm^2		Passive region width (E_B-E_A),
			Critical	Passive	
Copper:					
Naval brass.....	Yes.....	No.....	11.1	7.0	0.034
Berylco 50.....	Yes.....	No.....	10.4	5.6	.221
Berylco 717.....	Yes.....	Yes.....	17.8	6.1	.303
70-30 cupronickel	Yes.....	No.....	14.7	5.9	.309
90-10 cupronickel	Yes.....	No.....	11.5	4.4	.213
Titanium:					
Ti50A.....	Yes.....	No.....	12.3	1.1	1.188
Ti0.2Pd.....	Yes.....	No.....	11.0	1.0	1.437
Ti6Al4V.....	Yes.....	No.....	10.8	.95	1.133
Ti6Al2Nb1TalMo...	Yes.....	No.....	9.3	.95	1.135

discussed without regard for possible interfering electrochemical reactions owing to solution species.

Selected polarization curves, plotted as log i versus potential (arbitrary units on both axes), are given in figures 6 and 7 to illustrate the performance of the copper and titanium alloys, respectively. Among the features they show are the activation potential, E_A, the least noble potential where passivity is maintained; the breakdown potential, E_B, marking the beginning of the transpassive region and the least noble potential where pitting and/or crevice corrosion will initiate; and the protection potential, E_{prot}, the least noble potential wherein pitting and/or crevice corrosion will propagate. These features have been labeled on the curve for Berylco 717 (fig. 6), but can be found on other curves in figures 6 and 7 as well.

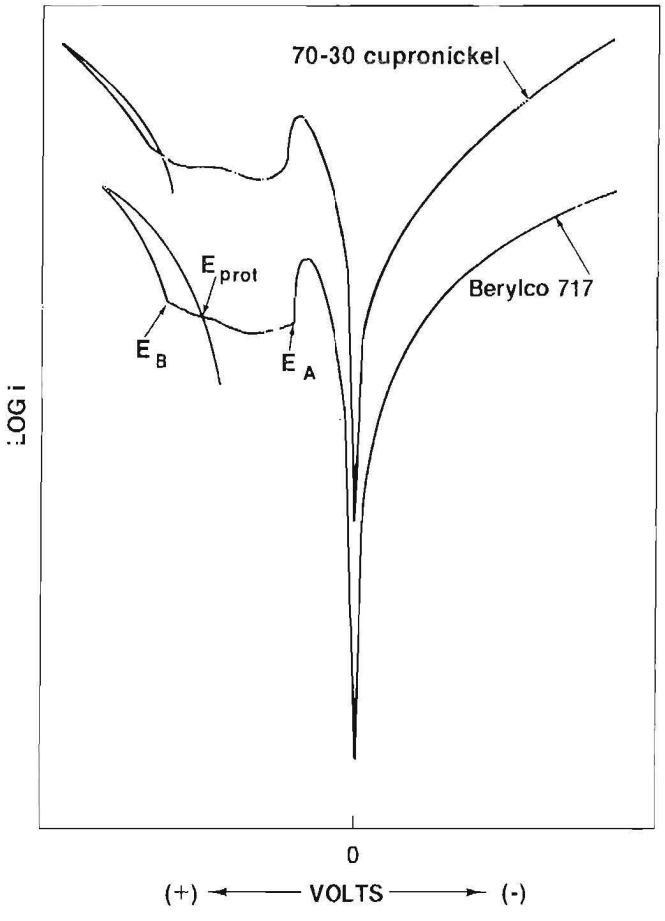

FIGURE 6. - Potentiodynamic polarization curves for 70-30 cupronickel and Berylco 717 exposed to wellhead brine at 215° C.

All of the copper and titanium alloys exhibited a region of active corrosion followed by a passive region at more noble potentials. Except for naval brass, the width of the passive region (E_B-E_A), for the copper alloys was 200 to 300 mV. Naval brass had a narrow passive region which may be due to its high (35.4 wt pct) zinc content. The width of the passive region for the titanium alloys was 1,100 to 1,400 mV and was characterized by several secondary peaks.

The point where the reverse scan crosses the forward scan is defined as the protection potential, E_{prot}, only when that point is at a potential less noble than the breakdown potential, E_B. Such a case is illustrated in figure 6 for Berylco 717. The attendant hysteresis in the polarization curve is associated with a range of potentials from E_{prot}, to E_B where the materials are considered susceptible to localized corrosion through the propogation of pits and crevice corrosion. Berylco 717 was the only copper alloy to exhibit this behavior in wellhead brine. None of the titanium alloys exhibited this behavior. However, Ti6Al4V and Ti50A were shown in the weight-loss measurements to be susceptible to crevice corrosion in wellhead brine, and Ti6Al4V was shown to be susceptible to pitting corrosion in wellhead brine.

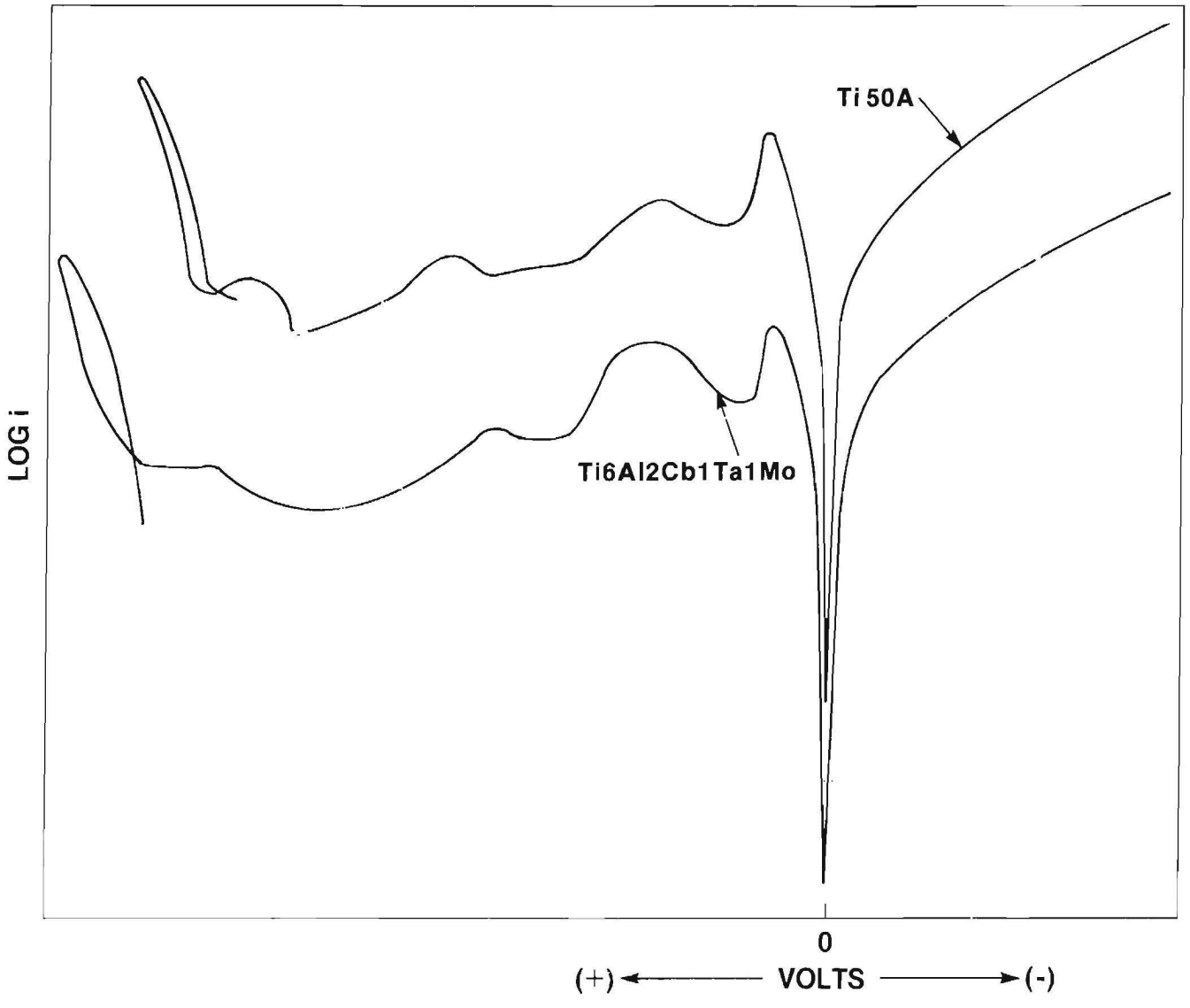

FIGURE 7. - Potentiodynamic polarization curves for Ti50A and Ti6Al2Cb1Ta1Mo exposed to wellhead brine at 215° C.

CONCLUSIONS

As a result of weight loss, pitting and crevice corrosion, U-bend stress corrosion, and electrochemical polarization measurements on several metals, and exposure tests on a high-temperature thermoplastic in brine and steam process environments produced from high-enthalpy hypersaline geothermal brine from geothermal well Magmamax No. 1, located at the Salton Sea KGRA in the Imperial Valley, Calif., the following conclusions were drawn.

1. Cadmium (and by extension cadmium coatings) and the 6061-T6 aluminum alloy are unsatisfactory for use in these environments owing to extremely high general corrosion rates and, in the case of the 6061-T6 aluminum alloy, severe pitting corrosion.

2. Molybdenum and niobium are resistant to general corrosion, pitting, and crevice corrosion in all of the environments.

3. Copper alloys corrode at rates that may be too high for use in the wellhead brine. The presence of iron in the alloy accelerates the corrosion. Neither

berylium, nickel, or zinc additions significantly affected the general corrosion rate of copper alloys in wellhead brine. Although the general corrosion rates were high, potentiodynamic polarization measurements indicated that the copper alloys, with the exception of Berylco 717, were not susceptible to pitting or crevice corrosion.

4. The titanium alloys are highly resistant to general corrosion in all of the brine and steam environments. Stress corrosion cracking was not observed in the titanium alloys exposed 45 days in these environments. Ti6Al4V was susceptible to pitting in the brine environments; whereas Ti50A and TiCode 12 were resistant to pitting in all of the environments. Ti50A, TiCode 12, and Ti6Al4V were each susceptible to crevice corrosion in some of the environments. Ti6Al4V and Ti6Al2NblTalMo were more resistant to general corrosion than Ti50A, but in long-term tests where pitting and, to a lesser extent, crevice corrosion are factors, the corrosion resistance of Ti6Al4V was less than that of Ti50A. The titanium alloys exhibit passive behavior over a broad range of potentials, 1.1 and 1.4 V.

5. The 40-pct-graphite-fiber-reinforced Ryton composite deteriorates readily in the wellhead brine and fails in all of the brine and steam process environments by the formation of cracks in the Ryton matrix. Cracking and, in wellhead brine, debonding of the graphite fibers probably resulted from the use of the composite in environments at temperatures above the maximum recommended temperature of 150° C.

6. Ryton coatings of 316L SS were generally adherent and appeared to withstand the temperatures and to perform well in all of the brine and steam process environments. Occasional blistering and edge chipping of the coatings should be corrected by more consistent coatings application. Ryton coatings should have useful applications in these environments.

REFERENCES

1. Babcock and Wilcox (Alliance, Ohio). Corrosion Resistance of Graphite Fiber Reinforced Polyphenylene Sulfide. Advanced Composites Dep. Tech. Data Sheet, November 1977, 1 p.

2. Blake, R. L. Extracting Minerals From Geothermal Brines: A Literature Study. BuMines IC 8638, 1974, 25 pp.

3. Carter, J. P., and S. D. Cramer. Field Stress Corrosion Tests in Brine Environments of the Salton Sea Known Geothermal Resource Area. Mater. Performance, v. 19, No. 9, 1980, pp. 13-16.

4. Carter, J. P., S. D. Cramer, and R. K. Conrad. Corrosion of Stainless Steels in the Geothermal Environments of the Salton Sea Known Geothermal Resource Area. Natl. Assoc. Corrosion Eng., Corrosion/81, Preprint 230, 1981, 15 pp.

5. Carter, J. P., F. X. McCawley, S. D. Cramer, and P. B. Needham, Jr. Corrosion Studies in Brines of the Salton Sea Geothermal Field. BuMines RI 8350, 1979, 35 pp.

6. Christopher, D. H., M. Stewart, and J. Rice. The Recovery and Separation of Mineral Values From Geothermal Brines (contract HO144104, Hazen Res., Inc.). BuMines OFR 81-75, 1975, 43 pp; NTIS PB 245 686.

7. Cramer, S. D. Estimation of the Slope of Polarization Curves in the Vicinity of the Corrosion Potential. J. Electrochem. Soc., v. 126, No. 6, 1979, pp. 891-893.

8. Cramer, S. D., and J. P. Carter. Corrosion in Geothermal Brines of the Salton Sea Known Geothermal Resource Area. Ch. in Geothermal Scaling and Corrosion, ed. by L. D. Casper and T. R. Pinchback. ASTM STP 717, 1980, pp. 113-141.

9. Cramer, S. D., and J. P. Carter. Laboratory Corrosion Studies in Low- and High-Salinity Geobrines of the Imperial Valley, Calif. BuMines RI 8415, 1980, 30 pp.

10. Cramer, S. D., and P. B. Needham, Jr. Linear Polarization Measurements at High Temperatures in Hypersaline Geothermal Brines. BuMines RI 8308, 1978, 15 pp.

11. Hammer, N. E. Corrosion Data Survey. Nat. Assoc. Corrosion Eng., Houston, Tex., 5th ed., 1974, p. X.

12. Hazen Research, Inc. The Recovery and Separation of Mineral Values from Geothermal Brines. Final Rep., HRZ Proj. 1370-01, June 1975, 39 pp.; available for consultation at BuMines, Avondale, Md.

13. McCawley, F. X., S. D. Cramer, W. D. Riley, J. P. Carter, and P. B. Needham, Jr. Corrosion of Materials and Scaling in the Low-Salinity East Mesa Geothermal Brines. BuMines RI 8504, 1981, 17 pp.

14. Phillips Chemical Co. (Bartlesville, Okla.). High Temperature and Corrosion Resistant Coatings of Ryton Polyphenylene Sulfide. Tech. Service Memorandum 275, February 1978, 7 pp.

15. _____. Ryton Polyphenylene Sulfide for Injection Molding. Tech. Services Memorandum 258, August 1973, 4 pp.

16. Sample, C. H., and E. C. Bertucio. Cadmium. Ch. 10 in Corrosion Resistance of Metals and Alloys, ed. by F. L. LaQue and H. R. Copson. Reinhold, New York, 1963, pp. 250-253.

17. Schultze, L. E., and D. J. Bauer. Operation of a Mineral Recovery Unit of Brine From the Salton Sea Known Geothermal Resource Area. BuMines RI 8680, 1982, 12 pp.

18. Syrett, B. C., D. D. MacDonald, H. Shih, and S. S. Wing. Corrosion Chemistry of Geothermal Brines. Stanford Res. Inst., Menlo Park, Calif., pt. 2, Dec. 16, 1977, p. 25.

19. Urbanek, M. W., C. D. Hornburg, and B. Lindal. Research on a Geothermal Mineral Extraction Complex. Phase 1. Preliminary Technical and Economic Assessment (contract JO275091, DSS Eng., Inc.). BuMines OFR 51-79, 1978, 204 pp.

☆U.S. GOVERNMENT PRINTING OFFICE: 1983-605-015/55

INT.-BU.OF MINES,PGH.,PA. 27000